

# SIMPLIFIED ANALYTICAL APPROACH TO THE BEAM RIPPLE GENERATION MECHANISM OF THE J-PARC MR SLOW EXTRACTION BEAMS

Y. Shirakabe\*, Institute of Particle and Nuclear Studies, KEK, Tsukuba, Japan

## Abstract

The 30 GeV proton beams are being stably extracted at the J-PARC Main Ring slow extraction system and delivered to the downstream Hadron Experimental Facilities, however presently, the large beam ripples deteriorate the beam spill qualities, while the ripple generation mechanisms are still not well understood yet.

In order to obtain better understandings on how such serious ripples are being generated in MR, a simplified analytical approach is taken, and some of the so far obtained results are presented.

The origin of the beam ripples can mainly be attributed to the magnetic field ripples of the main bending and quadrupole magnets of the MR. The simplified model of the magnet circuit allows the analytical solution with the ramp pattern magnet current. The dependence of the magnetic field ripples on the circuit parameters is discussed.

## INTRODUCTION

Beam ripples have been critically important in proton synchrotron operations for more than half a century since the invention of synchrotrons [1], and are still one of the hardest problems for today's J-PARC Main Ring beams. In the present MR slow extraction operations, for example [2], the beam spills are mainly composed of sharp spikes, as is shown in Figure 1, and they are found to be difficult to improve the spill shape even after the various ripple correction systems are turned on. The bottom of the spill in Fig. 1 is completely blackened by the spikes with various frequency component ripples ranging from tens to thousands Hz. The MR spill shapes are clearly worse

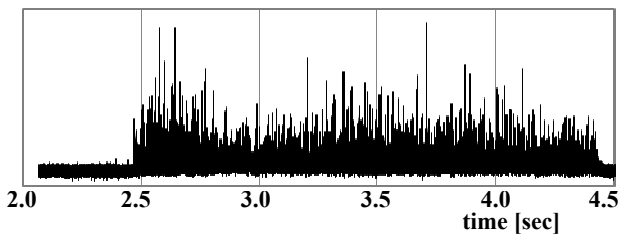


Figure 1: An example of the J-PARC MR slow extraction spills. The spill feedback systems of EQ and RQ, and the transverse RF are applied on the debunched MR beam [2].

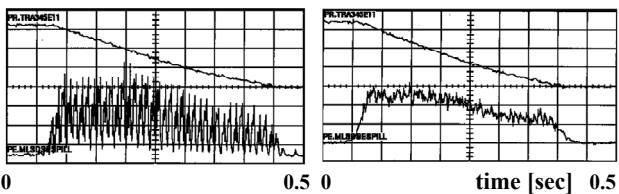


Figure 2: CERN PS slow extraction spills before (left) and after (right) the ripple correction system is turned on [3].

\*yoshihisa.shirakabe@kek.jp

compared to, for example, those of CERN PS in Figure 2 where the spills have clearer bottoms even without corrections.

The origins of beam ripples have been searched for years as is, for example, described in [4]. In the present MR case, the biggest source of the beam ripples is supposed to be the magnetic field ripples of the main dipole and quadrupole magnets. Since the beam ripples contain lots of frequency components that cannot necessarily be explained to be originated from the magnet power supplies [2], the mechanism on how the ripples with various frequency components are generated in the magnet circuit systems should be investigated.

In order to approach the better understanding on how the various ripples are generated in the MR magnet circuits, a simplified circuit model with a ramp pattern current is analytically solved, and the dependence of the ripples as a function of circuit parameters as inductance, capacitance, a ramp rate etc., is discussed.

## RAMP PATTERN OF MAGNET CURRENT

The dipole and quadrupole magnet currents in the proton synchrotrons ramp up and down in accordance with the proton acceleration cycles  $T_0$ , as is shown in Figure 3. The beam is injected at the flat-bottom current  $I_B$ , accelerated to the flat-top current  $I_T$ , and then extracted.

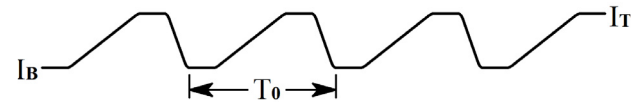


Figure 3: A typical magnet current ramp pattern with a cycle  $T_0$ , a flat-bottom current  $I_B$ , and a flat-top current  $I_T$ .

A magnet current ramps up from  $I_B$  to  $I_T$  as is shown in Figure 4. At first period of time [0], the current is  $I_B$ . The next period [1] is the smoothing time  $T_S$  where the current starts to swing up at  $t_B$  for  $T_S$  in parabolic curve. After  $t_B+T_S$  the current increases linearly during the period [2].

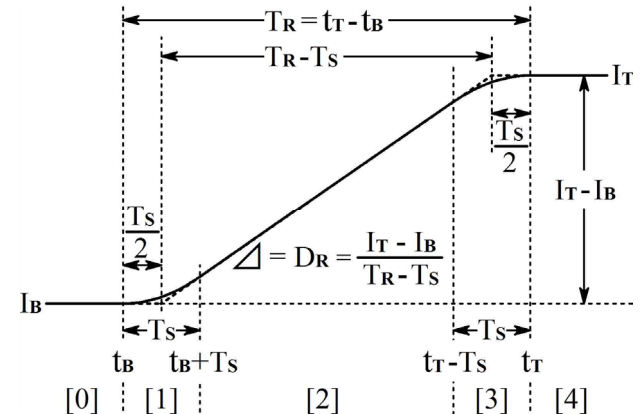


Figure 4: A magnet current ramp from  $I_B$  to  $I_T$ . The current swings up and back at [1] and [3], respectively, in parabolic curves in order to avoid sudden current changes.

The current starts to swing back at  $t_T - T_S$  for  $T_S$  in the period [3], again in parabola. At  $t_T$  the current reaches  $I_T$ , the period [4]. Due to the parabolic curve, the derivative  $D_R$ , i.e. the ramp rate of the magnet current, becomes

$$D_R = \frac{I_T - I_B}{T_R - T_S}, \quad \text{where } T_R = t_T - t_B \quad (1)$$

Accordingly, the magnet current as a function of time,  $I_0(t)$ , becomes as follows: At the period [0],  $I_0(t) \equiv I_B$ , and at the period [4],  $I_0(t) \equiv I_T$ . At the ramp periods [1], [2], and [3],

$$[1] I_0(t) = I_B + \frac{D_R (t - t_B)^2}{2}, \quad \dot{I}_0(t) = \frac{D_R}{T_S} (t - t_B) \quad (2)$$

$$[2] I_0(t) = I_B + D_R \left\{ t - \left( t_B + \frac{T_S}{2} \right) \right\}, \quad \dot{I}_0(t) = D_R \quad (3)$$

$$[3] I_0(t) = I_T - \frac{D_R (t_T - t)^2}{2}, \quad \dot{I}_0(t) = \frac{D_R}{T_S} (t_T - t) \quad (4)$$

### SIMPLIFIED CIRCUIT MODEL

Each dipole or quadrupole magnet system, called a family, has several to tens of magnet units connected in series by bus bars or cables. In Table 1 shows the families for the J-PARC MR. Each magnet unit, as well as each connection part, has its own inductance, resistance, and capacitance. The schematic circuit model of one magnet family, consequently, can be expressed as Figure 5, where the circuit contains  $N$  components which may be either the magnets or the connections. The current source  $I_0(t)$  outputs the ramp current which is mathematically ideal with no ripples as is defined in (2) to (4).

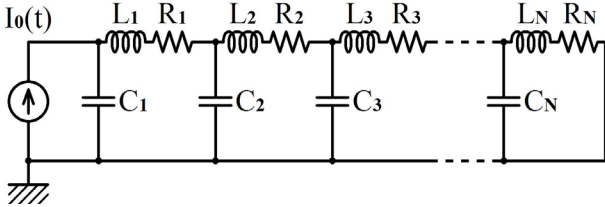


Figure 5: The schematic circuit model of one magnet family. The  $N$  components include both the magnets and the connections. The current source  $I_0(t)$  supplies the ramp current.

The current  $I_0(t)$  mainly flow through  $L_1, R_1, \dots, L_N, R_N$ , with fractional currents branching out at  $C_1, \dots, C_N$ . At  $n$ th component ( $n: 1$  to  $N$ ), the branch current to  $C_n$  represents the oscillation with the circuit inductance, i.e. the LC oscillation, with the amplitude that positively correlates with  $C_n$ . This LC oscillation is the magnet field ripple itself. The large capacitance generates the large ripple current.

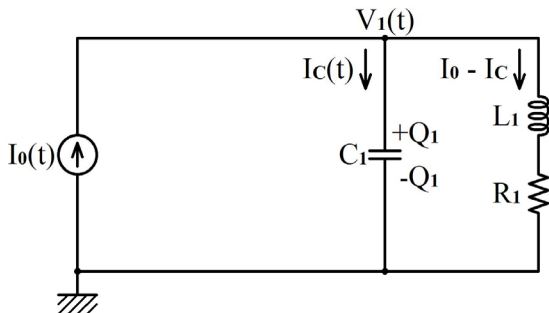


Figure 6: The simplified circuit model with a single load.

Solving the Fig. 5 circuit directly is too complicated and does not necessarily gives good insights on the circuit behaviour with respect to such parameters as inductance, capacitance, and the ramp rate. Instead, starting with the single load with  $L_1, R_1$ , and  $C_1$ , as is shown in Figure 6, the circuit behaviour becomes much simpler to understand.

### CIRCUIT EQUATIONS

In the Fig 6, the electric charge  $Q_1$  stored on  $C_1$  is

$$Q_1(t) = C_1 \cdot V_1(t) \quad (5)$$

Since the  $C_1$  current  $I_c(t)$  is the time derivative of  $Q_1$ ,

$$I_c(t) = \dot{Q}_1(t) = C_1 \cdot \dot{V}_1(t) \quad (6)$$

Using  $I_0(t)$  and  $I_c(t)$ , the potential  $V_1(t)$  is

$$V_1(t) = L_1(\dot{I}_0 - \dot{I}_c) + R_1(I_0 - I_c) \quad (7)$$

Substituting  $\dot{V}_1(t)$  in (6) by (7), the equation for  $I_c(t)$  is obtained as follows:

$$\ddot{I}_c + 2\lambda_1 \dot{I}_c + \omega_1^2 I_c = \ddot{I}_0 + 2\lambda_1 \dot{I}_0 \quad (8)$$

where  $\lambda_1$  and  $\omega_1$  are the basic circuit constants defined as

$$\lambda_1 = \frac{R_1}{2L_1} \text{ [1/sec]: damping constant,} \quad (9)$$

$$\omega_1 = \frac{1}{\sqrt{L_1 C_1}} \text{ [rad/sec]} \quad (10)$$

: angular frequency of LC oscillation.

The implications of the constants  $\lambda_1$  and  $\omega_1$  will be mentioned in the next section. The equation (8) is a constant coefficient second-order ordinary differential equation for the unknown function  $I_c(t)$ . The right side of (8) is obtained with the known function  $I_0(t)$  defined by (2) to (4). The general solution of (8) can be obtained as a sum of following (a) and (b).

(a) The general solution of (8)'s homogeneous equation:

$$\ddot{I}_c + 2\lambda_1 \dot{I}_c + \omega_1^2 I_c = 0 \quad (11)$$

(b) The particular solution of the nonhomogeneous equation (8) (12)

The solution of (8) for [1] to [4] is obtained as follows.

Table 1: J-PARC MR dipole & quadrupole magnet families. The magnet units marked in red are connected by shielded cables, resulting in large cable capacitance [5].

	N	Length	L	R	C	Cable	
						units	Total
BM1	17	5.85	103.5	42.52	50.0	2920	3770
BM2	16	5.85	103.5	42.52	50.0	3020	3820
BM3	16	5.85	103.5	42.52	50.0	3200	4000
BM4	16	5.85	103.5	42.52	50.0	3170	3970
BM5	16	5.85	103.5	42.52	50.0	2880	3680
BM6	16	5.85	103.5	42.52	50.0	2860	3660
QDN	48	1.86	70.5	39.90	22.3	2650	3720
QFN	48	1.56	59.7	34.60	18.7	2710	3608
QFX	48	1.26	48.9	30.10	15.1	2360	3085
QDX	27	1.66	63.3	36.00	19.9	2440	2977
QFR	9	1.76	63.3	38.30	21.1	3120	3310
QDR	6	1.86	70.3	39.90	22.3	640	774
QDT	6	1.86	67.7	39.60	22.3	490	624
QDS	6	1.66	59.9	36.30	19.9	490	609
QFT	6	1.46	53.0	33.10	17.5	500	605
QFS	6	1.26	48.8	30.10	15.1	510	601
QFP	6	0.86	32.5	23.25	10.3	720	782

## DAMPED OSCILLATION SOLUTION

The general solution of the homogeneous equation (11) is

$$I_C(t) = J_1 \cos(\sqrt{1-\varepsilon} \cdot \omega_1 t - \varphi_1) \cdot e^{-\lambda_1 t} \quad (13)$$

where  $J_1$  and  $\varphi_1$  are the arbitrary constants of integration that should be obtained by the initial conditions of the time periods [0] to [4], and  $\varepsilon$  is

$$\varepsilon = \left(\frac{\lambda_1}{\omega_1}\right)^2. \quad (14)$$

The solution  $I_C(t)$  behaves as the damped oscillation with the damping factor  $\lambda_1$  and the angular frequency  $\omega_1$ .

If the load is assumed, from Table 1, to have

$$L_1 = 10 \text{ mH}, R_1 = 10 \text{ m}\Omega, C_1 = 10 \text{ nF}, \quad (15)$$

then  $\lambda_1$  and  $\omega_1$  become

$$\lambda_1 = \frac{R_1}{2L_1} = 0.5 [1/\text{sec}], \quad t_d \equiv \frac{1}{\lambda_1} = 2 [\text{sec}] \quad (16)$$

$$\omega_1 = \frac{1}{\sqrt{L_1 C_1}} = 10^5 \left[\frac{\text{rad}}{\text{sec}}\right], \quad f_1 \equiv \frac{\omega_1}{2\pi} = 16 [\text{kHz}]. \quad (17)$$

If the load is assumed to be 10 times bigger than (15) as

$$L_1 = 100 \text{ mH}, R_1 = 100 \text{ m}\Omega, C_1 = 100 \text{ nF}, \quad (18)$$

then  $\lambda_1$  is the same as (16), and  $\omega_1$  becomes

$$\omega_1 = 10^4 [\text{rad/sec}], \quad f_1 = 1.6 [\text{kHz}]. \quad (19)$$

As the examples (15) and (18) show, the oscillations damp slowly, with the damping time  $t_d = 2\text{sec}$ . If the condition  $L_1 \propto R_1$  roughly holds in different size systems, then the slow damping characteristic also always holds.

The oscillation frequency  $f_1$  changes in inverse proportion to the load size as are shown in (17) and (19). If the condition  $L_1 \propto C_1$  roughly holds, the oscillation frequencies become lower in the bigger magnet systems.

In the realistic magnet systems in any size,  $\varepsilon$  defined in (14) is generally a small number;

$$\varepsilon \ll 1. \quad (20)$$

## SOLUTIONS IN PERIODS [1] TO [4]

The general solution of (8) is obtained as a sum of the particular solution of (8) and the general solution (13). The former can be obtained with  $I_0(t)$  at the ramp periods [1] to [4]. Unknown constants of integration,  $J_1$  and  $\varphi_1$ , can be obtained by applying the initial conditions.

**Solution in the period [1] ( $t_B \leq t < t_B + T_S$ ):**

In the period [1],  $\dot{I}_0(t)$  and  $\ddot{I}_0(t)$  are, from (2),

$$\dot{I}_0(t) = \frac{D_R}{T_S} (t - t_B), \quad \ddot{I}_0(t) = \frac{D_R}{T_S}. \quad (21)$$

With (21), the right side of (8) becomes

$$\ddot{I}_0 + 2\lambda_1 \dot{I}_0 = \frac{D_R}{T_S} + 2\lambda_1 \frac{D_R}{T_S} (t - t_B). \quad (22)$$

From (22), the particular solution  $I_C(t)$  in the left side of (8) can be assumed as a first-degree function of  $t$ , such as

$$I_C(t) = a + b(t - t_B). \quad (23)$$

Substituting (23) for the left side of (8),  $I_C(t)$  becomes

$$I_C(t) = \frac{1-4\varepsilon}{\omega_1^2} \frac{D_R}{T_S} + \frac{2\lambda_1}{\omega_1^2} \frac{D_R}{T_S} (t - t_B). \quad (24)$$

From (24) and (13), the general solution of (8) can be obtained, while substituting  $t$  to  $t - t_B$  in (13), as

$$I_C(t) = \frac{1-4\varepsilon}{\omega_1^2} \frac{D_R}{T_S} + \frac{2\lambda_1}{\omega_1^2} \frac{D_R}{T_S} (t - t_B) + J_1 \cos(\sqrt{1-\varepsilon} \cdot \omega_1 (t - t_B) - \varphi_1) e^{-\lambda_1 (t - t_B)}. \quad (25)$$

The initial conditions for (25) is that the expression (25) in the period [1] smoothly connects to that in [0], i.e.,

$$I_C(t_B) = 0, \quad \dot{I}_C(t_B) = 0. \quad (26)$$

Applying the condition (26) on (25),  $J_1$  and  $\varphi_1$  are obtained, and the expression of  $I_C(t)$  for the period [1] is;

$$I_C(t) = \frac{D_R}{\omega_1^2 T_S} \left\{ (1-4\varepsilon) + 2\lambda_1 (t - t_B) - \frac{1}{\sqrt{1-\varepsilon}} \cos(\sqrt{1-\varepsilon} \cdot \omega_1 (t - t_B) - \varphi_1) e^{-\lambda_1 (t - t_B)} \right\} \quad (27)$$

$$\varphi_1 = \text{Tan}^{-1} \frac{3-4\varepsilon}{1-4\varepsilon} \sqrt{\frac{\varepsilon}{1-\varepsilon}}. \quad (28)$$

It is easily confirmed that  $I_C(t)$  in (27) satisfies (26).

The right side of (27) is composed of 3 terms; the constant term  $(1-4\varepsilon)$ , the term proportional to the elapsed time  $2\lambda_1 (t - t_B)$ , and the damped oscillation term.

$I_C(t)$  obeys the proportional expression as

$$I_C(t) \propto \frac{D_R}{\omega_1^2 T_S} = L_1 C_1 \frac{D_R}{T_S} \quad (29)$$

This relation is essentially important. The magnitude of the damped oscillation is proportional to the circuit inductance and capacitance  $L_1, C_1$ , and the ramp rate  $D_R$ .

**Solution in the period [2] ( $t_B + T_S \leq t < t_T - T_S$ ):**

In the period [2],  $\dot{I}_0(t)$  and  $\ddot{I}_0(t)$  are, from (3),

$$\dot{I}_0(t) = D_R, \quad \ddot{I}_0(t) = 0. \quad (30)$$

The initial conditions in the period [2] is

$$\begin{cases} I_C(t_B + T_S) = I_C(t_B + T_S) \text{ in [1]}(27) \\ \dot{I}_C(t_B + T_S) = \dot{I}_C(t_B + T_S) \text{ in [1]}(27) \end{cases} \quad (31)$$

From (30) and (31),  $I_C(t)$  is solved as

$$I_C(t) = \frac{D_R}{\omega_1^2 T_S} \left\{ 2\lambda_1 T_S + \frac{S_2}{\sqrt{1-\varepsilon}} \cdot \cos(\sqrt{1-\varepsilon} \cdot \omega_1 (t - (t_B + T_S)) - \varphi_2) e^{-\lambda_1 (t - (t_B + T_S))} \right\} \quad (32)$$

$$S_2 = \sqrt{1 - 2 \cos(\sqrt{1-\varepsilon} \cdot \omega_1 T_S) e^{-\lambda_1 T_S} + e^{-2\lambda_1 T_S}} \quad (33)$$

$$\varphi_2 = \text{Tan}^{-1} \frac{\sin \varphi_1 + \sin(\sqrt{1-\varepsilon} \cdot \omega_1 T_S - \varphi_1) e^{-\lambda_1 T_S}}{\cos \varphi_1 - \cos(\sqrt{1-\varepsilon} \cdot \omega_1 T_S - \varphi_1) e^{-\lambda_1 T_S}}. \quad (34)$$

The solution (32) satisfies the initial conditions (31) as is easily checked, and keeps the relation (29).

**Solution in the period [3] ( $t_T - T_S \leq t < t_T$ ):**

In the period [3],  $\dot{I}_0(t)$  and  $\ddot{I}_0(t)$  are, from (4),

$$\dot{I}_0(t) = \frac{D_R}{T_S} (t_T - t), \quad \ddot{I}_0(t) = -\frac{D_R}{T_S}. \quad (35)$$

The initial conditions in the period [3] is

$$\begin{cases} I_C(t_T - T_S) = I_C(t_T - T_S) \text{ in [2]}(32) \\ \dot{I}_C(t_T - T_S) = \dot{I}_C(t_T - T_S) \text{ in [2]}(32) \end{cases} \quad (36)$$

From (35) and (36),  $I_C(t)$  is solved as

$$I_C(t) = \frac{D_R}{\omega_1^2 T_S} \left\{ -(1-4\varepsilon) + 2\lambda_1 (t_T - t) + \frac{S_3}{\sqrt{1-\varepsilon}} \cdot \cos(\sqrt{1-\varepsilon} \cdot \omega_1 (t - (t_T - T_S)) - \varphi_3) e^{-\lambda_1 (t - (t_T - T_S))} \right\} \quad (37)$$

$$S_3 = \sqrt{1 - 2 S_2 \cos(\sqrt{1-\varepsilon} \cdot \omega_1 (T_R - 2T_S) + \varphi_1 - \varphi_2) \cdot e^{-\lambda_1 (T_R - 2T_S)} + S_2^2 \cdot e^{-2\lambda_1 (T_R - 2T_S)}} \quad (38)$$

$$\varphi_3 = \text{Tan}^{-1} \frac{\left( \begin{array}{l} \sin \varphi_1 \\ -S_2 \cdot \sin(\sqrt{1-\varepsilon} \cdot \omega_1(T_R - 2T_S) - \varphi_2) \\ \cdot e^{-\lambda_1(T_R - 2T_S)} \end{array} \right)}{\left( \begin{array}{l} \cos \varphi_1 \\ +S_2 \cdot \cos(\sqrt{1-\varepsilon} \cdot \omega_1(T_R - 2T_S) - \varphi_2) \\ \cdot e^{-\lambda_1(T_R - 2T_S)} \end{array} \right)} \quad (39)$$

The solution (37) satisfies (36), and keeps the relation (29).

**Solution in the period [4] ( $t_T \leq t$ ) :**

In the period [4],  $\dot{I}_0(t)$  and  $\ddot{I}_0(t)$  are

$$\dot{I}_0(t) = \ddot{I}_0(t) = 0 \quad (40)$$

The initial conditions in the period [4] is

$$\begin{cases} I_C(t_T) = I_C(t_T) \text{ in [3](37)} \\ \dot{I}_C(t_T) = \dot{I}_C(t_T) \text{ in [3](37)} \end{cases} \quad (41)$$

From (40) and (41),  $I_C(t)$  is solved as

$$I_C(t) = \frac{D_R}{\omega_1^2 T_S} \frac{S_4}{\sqrt{1-\varepsilon}} \cos(\sqrt{1-\varepsilon} \cdot \omega_1(t - t_T) - \varphi_4) \cdot e^{-\lambda_1(t-t_T)} \quad (42)$$

$$S_4 = \sqrt{1 - 2S_3 \cos(\sqrt{1-\varepsilon} \cdot \omega_1 T_S + \varphi_1 - \varphi_3) e^{-\lambda_1 T_S} + S_3^2 \cdot e^{-2\lambda_1 T_S}} \quad (43)$$

$$\varphi_4 = \text{Tan}^{-1} \frac{\sin \varphi_1 + S_3 \sin(\sqrt{1-\varepsilon} \cdot \omega_1 T_S - \varphi_3) e^{-\lambda_1 T_S}}{\cos \varphi_1 - S_3 \cos(\sqrt{1-\varepsilon} \cdot \omega_1 T_S - \varphi_3) e^{-\lambda_1 T_S}} \quad (44)$$

The solution (42) satisfies (41), and keeps the relation (31).

## COMPARISON TO THE SIMULATIONS

The first part of the solution  $I_C(t)$  is plotted in Figure 7. The parabola smoothing time  $T_S = 100\text{msec}$  and the circuit parameters of (15) are assumed. In the lower two figures, the analytical solutions (black) and the LTSpice simulation results (red) are shown. They agree well, suggesting the validity of the analytical solutions.

As is shown in (16), the ripple  $I_C(t)$  damps slowly. In the time range of Fig. 7, the amplitude is almost constant.

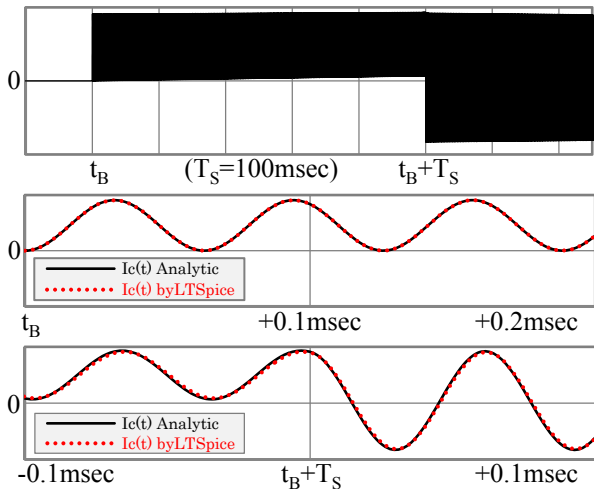


Figure 7: Top: The obtained ripple current  $I_C(t)$  plotted for 150msec from the beginning of the current ramp  $t_B$ . Middle and bottom: The expanded plots for the 0.2msec period at  $t_B$  and  $t_B + T_S$ . The circuit parameters of (15) are assumed, where one cycle becomes 0.063msec.

## DAMPED OSCILLATION AMPLITUDES

In the parabola periods [1] and [3], the solutions of  $I_C(t)$  in (27) and (37) contain the constant term  $(1 - 4\varepsilon)$  and the term proportional to the elapsed time. In the linear ramp period [2], the constant term  $2\lambda_1 T_S$  is included in (32).

Apart from those terms, all the solutions from [1] to [4], marked in blue, contain the damped oscillation terms. If  $\varepsilon$  and  $\varphi_n$  ( $n: 1$  to  $4$ ) are ignored due to their relatively small values, the damped oscillation term can be characterized by

$$S_n \cos \omega_1 \Delta t \cdot e^{-\lambda_1 \Delta t} \quad (45)$$

where  $S_n$  is the specific amplitude and  $\Delta t$  is the elapsed time of each period.

In the expressions of  $S_n$ , (33), (38), and (43), the cosine values are between -1 and 1. Hence the ranges of  $S_n$  become

$$\begin{aligned} 1 - e^{-\lambda_1 T_S} &\leq S_2 \leq 1 + e^{-\lambda_1 T_S} \\ |1 - S_2 e^{-\lambda_1(T_R - 2T_S)}| &\leq S_3 \leq 1 + S_2 e^{-\lambda_1(T_R - 2T_S)} \end{aligned} \quad (46)$$

$$|1 - S_3 e^{-\lambda_1 T_S}| \leq S_4 \leq 1 + S_3 e^{-\lambda_1 T_S}$$

If, for example,  $\lambda_1 = 0.5\text{sec}^{-1}$  and  $T_S = 0.1\text{sec}$ ,  $e^{-\lambda_1 T_S}$  is close to unity because of the slow damping, and  $S_2$  is

$$0.0488 \leq S_2 \leq 1.9512 \quad (47)$$

The value  $S_2$  largely changes by a factor of up to 40 if the cosine value in (33),  $\cos(\sqrt{1-\varepsilon} \cdot \omega_1 T_S)$ , changes. The same property is applied to  $S_3$ ,  $S_4$ , and to all the amplitudes in the following ramp cycles in Fig. 3.

In the J-PARC MR slow beam extractions, it is generally observed that the spill shapes, as is shown in Fig. 1, change every cycle to cycle of the MR acceleration. Sensitive fluctuations of  $S_n$  in connection to the cosine values will be the origin of this irreproducibility.

## CIRCUIT PARAMETER DEPENDANCE

As are shown in the solutions (27), (32), (37), and (42), the ripple current  $I_C(t)$  always has the form of

$$I_C(t) = \frac{D_R}{\omega_1^2 T_S} \left\{ \dots \right\} \quad (48)$$

where the terms inside the parentheses  $\{ \}$  are the dimensionless numbers in the order of unity and define the dependence of ripple as a function of time.

Outside of the parentheses  $\{ \}$  is the factor that signifies the magnitude of the ripple. Here this factor is defined as

$$I_{C0} \equiv \frac{D_R}{\omega_1^2 T_S} = L_1 C_1 \frac{D_R}{T_S} \quad (49)$$

As is seen from (49), the ripple magnitude  $I_{C0}$  is proportional to the circuit inductance  $L_1$ , the capacitance  $C_1$ , the ramp rate  $D_R$ , and inverse of the parabola smoothing time  $T_S^{-1}$ .

In the originally designed requirements of MR, the expected current ripple is  $\sim 10^{-6}$  at the extraction [7]. The maximum designed bending magnet current is  $\sim 3000$  A at 50 GeV. The corresponding ripple current is

$$3000 \cdot 10^{-6} = 3 \text{ mA} \quad (50)$$

Hence the ripple current  $I_{C0}$  should be in the order of mA.

Assuming simple numbers for example, from Table 1, as follows,

$$\begin{aligned} L_1 &\sim 1000 \text{ mH}, C_1 \sim 1000 \text{ nF}, \\ D_R &\sim 1000 \text{ A/sec}, T_S = 0.1\text{sec}, \end{aligned} \quad (51)$$

then the ripple current  $I_{C0}$  becomes

$$I_{C0} = L_1 C_1 D_R / T_S \sim 10 \text{ mA} \quad (52)$$

The estimation of (52) shows that, although the expression of  $I_{C0}$  is based on the simplified circuit, Fig. 6, the derived LC oscillation current formula (49) properly represents the magnitude of the ripple current.

In the realistic MR case at present, however, the total capacitance of each magnet family is several times bigger than the sum of magnet capacitance. The cables used for the electrical connections of the magnets bring large capacitance into the circuit, as is shown in Table 1. The resulted ripple in (49) will be  $I_{C0} \sim 30\text{mA}$  with  $C_1 \sim 3000\text{nF}$ .

The beam ripple influence with the large capacitance is particularly severe in the injection periods when the beam size is large and the majority of the beam power loss is occurring. If the ramp down rate just before the injection period is assumed to be bigger than the ramp up rate as  $D_R = 2000 \text{ A/sec}$ , and  $C_1 \sim 3000\text{nF}$ , then  $I_c(t) \sim 60 \text{ mA}$ . The bending magnet current at the injection period is  $\sim 200\text{A}$ , hence the ripple rate is  $\sim 60\text{mA}/200\text{A} = 3 \times 10^{-4}$ . With an uncontrolled  $T_S$ , it may even reach  $10^{-3}$ .

### BUS BAR AND CABLE CAPACITANCE

Since the inductance is mainly defined by the machine dimensions such as magnet apertures or power line lengths, it's impossible to reduce  $L_1$  in the  $I_{C0}$ .formula (49). The only possible way to lower the ripple is to reduce the capacitance of the entire circuit.

In order to fulfil this critical requirement, bus bar connections are commonly employed in the major proton synchrotrons, as are described in, for example, [3] and [6]. In bus bars, the capacitance per unit length is in general tens of times smaller than that of cables [8]. In fact, if the bus bar capacitance is estimated as co-axial conductors with an inner conductor radius  $r_i$  of 2cm and an outer conductor radius  $r_o$  of 0.5m, the capacitance per unit length  $C_0$  becomes

$$C_0 \equiv 2\pi\epsilon_0/\ln(r_o/r_i) \sim 17 \text{ nF/km} . \quad (53)$$

The assumed outer radius  $r_o$  may differ from place to place in the synchrotron tunnel, but  $C_0$  in (53) is generally insensitive to  $r_o$  when its size is assumed to be  $\geq 0.1\text{m}$ .

In contrast to bus bars, high current cables have  $r_o$  only  $\sim 20\%$  or so larger than  $r_i$ , resulting in a large factor of  $1/\ln(r_o/r_i) > 5$ . And there exists another factor multiplied, that is the relative permittivity of  $\epsilon' \sim 2.26$  for the crosslinked polyethylene insulation layer between the inner and outer conductors. As a result, the cable capacitance per unit length  $C_{\text{Cable}}$ , for example for the  $500 \text{ mm}^2$  shielded cables [9] used for the MR bending and quadrupole magnets, becomes

$$C_{\text{Cable}} \equiv 2\pi\epsilon'\epsilon_0/\ln(r_o/r_i) \sim 740\text{nF/km} . \quad (54)$$

The original design for the high current connection of the MR magnets is naturally by bus bars which have the same dimensions as the magnet's hollow conductors [8]. The design was kept for a while in the MR construction period [10] but later it was changed to the cables [11].

In the realistic case, the large cable capacitance is divided and scattered in the MR tunnel along with the magnets as in Figure 5, forming lots of minor current loops associated with the ripples of various LC oscillation frequencies. In the simplified treatment at present with a single load, the distributed feature of multiple loads is ignored. The expansion to the multiple element circuit is the next step subject and will be reported elsewhere.

### RAMP PARAMETER DEPENDANCE

As is seen from (49), the ripple current  $I_c(t)$  is related to the current ramp parameters as

$$I_c(t) \propto D_R/T_S . \quad (55)$$

This factor appears in the right side of the circuit equation (8),  $\ddot{I}_0 + 2\lambda_1\dot{I}_0$ , as is seen in (22). This feature holds in the circuits with multiple loads, although its proof is skipped in this article. It is only pointed out here that the proportional expression (55) always holds in any circuit.

### SUMMARY

The beam ripple generation mechanism in proton synchrotron magnet ramp currents is analytically investigated in a simplified circuit model.

It is revealed that the magnet current ripple is generated by the magnet current ramp itself, even if the ramp current as a function of time is mathematically ideal with no ripples. The magnitude of the resulting ripple current is proportional to the circuit capacitance and the ramp rate. The large capacitance and the faster ramp increase the ripples.

### ACKNOWLEDGMENT

The author would like to thank Associate Professor M. Tomizawa, Dr. T. Kimura, and Dr. T. Shimogawa for the fruitful discussions and encouragements. The author also would like to thank all the people involved in the MR slow extraction beam development for their timeless efforts.

### REFERENCES

- [1] V. I. Veksler et al., "The 10 BeV proton synchrotron of the Academy of Science USSR," Atomic Energy, Vol. 1, Num. 4 (1956) 469; <http://www.springerlink.com/content/t763155115r04167/>
- [2] M. Tomizawa et al., "PERFORMANCE OF RESONANT SLOW EXTRACTION FROM J-PARC MAIN RING," Proc. of IPAC'12, New Orleans, May 2012, to be published.
- [3] S. Gilardoni et al., "Fifty years of the CERN PS Synchrotron Volume I," CERN-2011-004 (2011) 103; <https://cdsweb.cern.ch/record/1359959>
- [4] L. Chapman et al., "OPERATION OF THE TEVATRON EXTRACTION SYSTEM," Proc. of PAC'85, Vancouver, May 1985, p. 3116; <http://cdsweb.cern.ch/record/897635>
- [5] Datasheet of Toshiba TMEIC Corporation as of 2009 measurements.
- [6] P. Zhang et al., "COMMON MODE NOISE ON THE MAIN TEVATRON BUS AND ASSOCIATED BEAM EMITTANCE GROWTH," Proc. of PAC'91, San Francisco, California, May 6-9, 1991, p. 93; [http://accelconf.web.cern.ch/AccelConf/p91/PDF/PAC1991\\_0093.PDF](http://accelconf.web.cern.ch/AccelConf/p91/PDF/PAC1991_0093.PDF)
- [7] M. Muto, "50 GeV Ring IGBT Power Supply and Ripples," Proc. of the Slow Extraction Meeting in Japan, Tanashi, Mar. 2000, KEK Proceedings 2002-15 (2003) p.131 (in Japanese).
- [8] M. Muto, private communications.
- [9] Hitachi Cable, Ltd. Cable Handbook: [http://www.hitachi-cable.co.jp/ICSFiles/cable/ecocable/em\\_6000v\\_ce\\_f.pdf](http://www.hitachi-cable.co.jp/ICSFiles/cable/ecocable/em_6000v_ce_f.pdf)
- [10] T. Oogoe, "J-PARC 50 GeV Proton Synchrotron Main Magnets Cablings," Proc. of the Meeting on the Technical Study at KEK, Tsukuba, Nov. 2006, KEK Proceedings2006-6 (2006) p.1 (in Japanese).
- [11] T. Oogoe, "STATUS AND SCHEDULE OF J-PARC 50GEV SYNCHROTRON (3)," Proc. of the 4th Annual Meeting of Particle Accelerator Society of Japan, Wako, Japan, Aug. 2007, p.221 (in Japanese), [http://www.pasj.jp/web\\_publish/pasj4\\_lam32/PASJ4-LAM32%20%28D%29/contents/PDF/WP/WP03.pdf](http://www.pasj.jp/web_publish/pasj4_lam32/PASJ4-LAM32%20%28D%29/contents/PDF/WP/WP03.pdf)